Supplementary Information

Anion-Competition Regulation of PbI_2 Frameworks for Two-Step Fabricated Perovskite Solar Cells

Qing Yao[a], Jianbing Zhu[a], Changshun Chen[ab], Guang Yang[a], Zhenhuang Su[c], Tingting Niu[a], Tengfei Pan[a], Kui Xu[a], Yingdong Xia[a], Xingyu Gao[c], Lingfeng Chao[a*], Yonghua Chen[a*]

[a]State Key Laboratory of Flexible Electronics (LoFE) & Institute of Advanced Materials (IAM), School of Flexible Electronics (Future Technologies), Nanjing Tech University (NanjingTech), Nanjing 211816, China.

[b]Frontiers Science Center for Flexible Electronics, Institute of Flexible Electronics (IFE) and Xi'an Institute of Biomedical Materials & Engineering, Northwestern Polytechnical University, 127 West Youyi Road, Xi'an 710072, China

[c]Shanghai Synchrotron Radiation Facility, Shanghai Institute of Applied Physics, Chinese Academy of Sciences, Shanghai 201204, P. R. China.

Qing Yao and Jianbing Zhu contribute equally.

Corresponding Authors

*E-mail: iamlfchao@njtech.edu.cn (L.C.)

*E-mail: iamyhchen@njtech.edu.cn (Y.C.)

‡ These authors contributed equally to this work.

Experimental section

Materials

Dehydrated ethanol (Sigma-Aldrich, anhydrous, 99%); methylamine solution (Sigma-Aldrich, 33 wt.% in absolute ethanol); 4-fluoro-phenethylammonium formate (4F-PEAFa, Suzhou LiWei Tech Co., Ltd, 99.5%); acetic acid (Sigma-Aldrich, anhydrous, 99%); formamidinium iodide (FAI, GreatCell Solar, 99.9%); methylamine chloride (MACl, GreatCell Solar, 99.9%); lead iodide (PbI_2, TCI, 98%); SnO_2 (Alfa Aesar); Spiro-OMeTAD (Liaoning Youxuan New Energy Technology Co., Ltd, 99.8%); chlorobenzene (CB, Sigma-Aldrich, 99.7%); fullerene-C_{60} (C_{60}, Liaoning Youxuan New Energy Technology Co., Ltd, 99.9%); bathocuproine (BCP, Suzhou LiWei Tech Co., Ltd, 99.9%); Bis(trifluoromethane)sulfonimide lithium salt (Li-TFSI, Sigma-Aldrich); isopropanol (IPA, Sigma-Aldrich, 99.5%); 2-Fluorophenylethylammonium Iodide (o-F-PEAI, Xi'anYuri Solar, 99%); 4-tertbutyl-pyridine (TBP, Sigma-Aldrich); molybdenum trioxide (MoO_3, Sigma-Aldrich, 99%); Ag (99.99%); MAAc refer to our previously reported work. All the materials were used as received without further purification.

Fabrication of perovskite Solar Cells

FTO glass substrates were cleaned with detergent, de-ionized water, acetone, and iso-propanol, in sequence, then treated with ultraviolet ozone for 15 min. The diluted SnO_2 nanoparticle solution (2.67 wt%) was deposited on FTO substrate at 4,000 rpm for 30 s, and then annealed at 150 °C for 30 min. For the fabrication of the perovskite film, a two-step deposition method was employed. First, the PbI_2 solution (400 mg/mL) in the

MAAc was printed on the SnO_2 layer by screen printing and annealed at 120 °C for 5 min. 8-32 mg 4F-PEAFa additives was added to PbI_2 solution in MAAc, printed on SnO_2 layer and annealed at 170 °C for 5 min. Subsequently, the FAI/MACl solution (90 : 9 mg/1 mL IPA) was coated on the PbI_2 film at 4000 rpm for 25 s and then annealed at 150 °C for 10 min. Then, o-P-PEAI solution (3 mg/mL in IPA) was spin-coated on the perovskite at 3000 rpm for 30 s. After, Spiro-OMeTAD in CB solution (72.6 mg/mL) with 17.5 mL of Li-TFSI (520 mg/mL in ACN) and 29 mL of TBP was deposited the perovskite layer by spin coating at 3,000 rpm for 30 s. Finally, MoO_3 (5 nm) and Ag (100 nm) were sequentially deposited on the hole transport layer under a high vacuum (vacuum is 1×10^{-4} Pa) at a rate of 0.01 and 0.1 nm/s, respectively. The screen-printed PbI_2 films were fabricated with a printing speed of 10 cm s^{-1}, a printing gap of 0.4 mm, a printing pressure of 0.27 MPa, a substrate temperature of 30 °C and a mesh count of 400.

Fabrication of perovskite Solar Modules

First, the P1 pattern is etched on the FTO using a picosecond laser marker. The SnO_2 layer is then deposited by spin-coating. The SnO_2 colloid precursor was diluted to 0.33% with deionized water. The FTO substrate was spin coated at 4000 rpm for 30 s and then annealed at 150 °C for 30 min. First, PbI_2 ink was screen printed on FTO/SnO_2 substrate with 400 mg/ml PbI_2 as raw material. 16 mg 4F-PEAFa additive was added to PbI_2 solution, printed on SnO_2 layer and annealed at 170 °C for 5 min. Subsequently, the FAI/MACl solution (90 : 9 mg/1 mL IPA) was coated on the PbI_2 film at 4000 rpm for 25 s and then annealed at 150 °C for 10 min. The printing speed is 10 cm s^{-1}, the

printing gap is 0.4 mm, the printing pressure is 0.25 MPa, the substrate temperature is 25 °C, and the mesh number is 400. Then, o-P-PEAI solution (3 mg/mL in IPA) was spin-coated on the perovskite at 3000 rpm for 30 s. The Spiro-OMeTAD solution was spun on the perovskite at 2500 rpm for 30 s. Line P2 was marked by laser marking near line P1, and finally line P3 was marked after MoO_3/Ag electrode deposition. P1 line scribbling rate is 500 mm s^{-1}, frequency is 100 kHz, power is 1.25 W. Line P2 has a scribbling rate of 600 mm s^{-1}, a frequency of 55 kHz, and a power of 0.40 W. The P3 line has a scribbling rate of 700 mm s^{-1}, a frequency of 55 kHz, and a power of 0.35 W. The widths of P1, P2 and P3 are 15 μm, 35 μm and 25 μm, respectively. The distances between P1-P2 and P2-P3 are 30 μm and 50 μm, respectively.

Characterizations

The X-ray diffraction (XRD) patterns were performed using Cu Ka radiation as the X-ray source by a Smart Lab diffractometer from Japan. The morphology of perovskite was characterized using scanning electron microscopy (SEM, S-4800, Hitachi). Surface topographies (AFM) were imaged using an atomic force microscope (Keysight 5500). Grazing-incidence wide-angle X-ray scattering (GIWAXS) was characterized at the beamline BL14B1 of the Shanghai Synchrotron Radiation Facility (SSRF). The sample was tested with an X-ray beam of l = 0.68877 Å at an incident angle of 0.50° for 400 s, and the scattered light was detected with MarCCD at a distance 746 mm vertically from the samples. Steady-state photoluminescence (PL) spectra and time-resolved photoluminescence (TRPL) were recorded on a Hitachi F-4600 fluorescence spectrophotometer. ultraviolet-visible (UV-vis) spectra were measured with a Varian

Cary5. ^{1}H and ^{13}C nuclear magnetic resonance (NMR) spectra were obtained using a JNM-ECZ400S/L1 magnetic resonance spectrometer (Nippon Electronics, Japan). Fourier transform infrared spectroscopy (FTIR) was performed by Thermo-Fisher Nicolet 6700 system. Time-resolved PL spectra were performed using an Edinburgh FS5-TCSPC system. PL mapping was carried out on a FILM300 system (TIME TECH SPECTRA) using a 405 nm excitation source. Transient photocurrent (TPC) measurement was performed with a system excited by a 532 nm (1000 Hz, 3.2 ns) pulse laser. Transient photovoltage (TPV) measurement was performed with the same system excited by a 405 nm (50 Hz, 20 ms) pulse laser. The electrochemical impedance spectra (EIS) were measured at an applied bias of open-circuit voltage (V_{OC}) with a frequency range from 10 kHz to 0.1 Hz and 20 Mv AC amplitude and the capacitance-voltage (C-V) measurement was swept from 0 V to 1.3 V at a fixed frequency under dark conditions. The C-V and EIS were measured by an electrochemical workstation (E4990A). The J-V characteristics of solar cells were measured at room temperature using a Keithley 2400 Source Meter under simulated sunlight from a solar simulator (SSF5-3A, EnliTech). The light intensity was calibrated to 100 mW cm^{-2} using a standard monocrystalline silicon cell.

Computational Details

All the calculations are carried out within the framework of density functional theory. The electrostatic potential (ESP) and binding energy calculations were carried out using the B3LYP functional in combination with the 6-311+G (d, p) basis set through the Gaussian 16 software package.[30] The adsorption energy and differential

charge density calculations are implemented in the Vienna Ab initio simulation package [31] using the project-enhanced plane wave method. The generalzied gradient approximation proposed by Perdew, Burke, and Ernzerhof is selected for the exchange-correlation potential.[32] The long ranges van der Waals interaction is described by the DFT-D3 approach.[33] The cut-off energy for plane wave is set to 500 eV. The energy criterion is set to 10^{-5} eV in iterative solution of the Kohn-Sham equation. A vacuum layer of 15 Å is added perpendicular to the sheet to avoid artificial interaction between periodic images. The Brillouin zone integration is performed using a 3x3x1 k-mesh. All the structures are relaxed until the residual forces on the atoms have declined to less than 0.03 eV/Å. In the iterative solution of the Kohn-Sham equation for static self-consistent calculation, the energy standard is set at 10^{-6} eV.

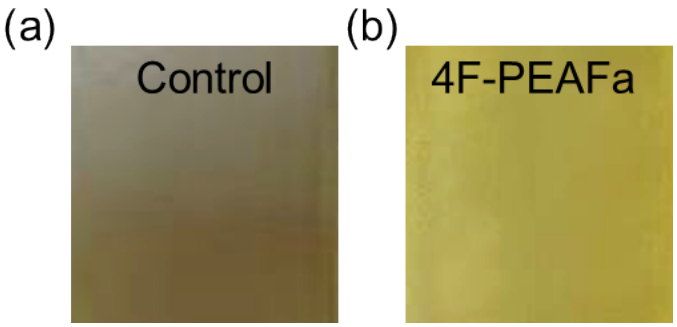

Fig. S1. Photos of (a) control and (b) 4F-PEAFa PbI_2 thin films.

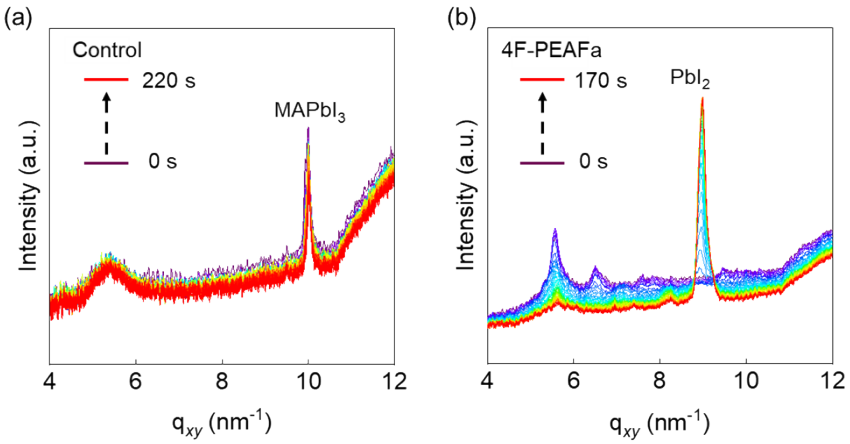

Fig. S2. 1D GIWAXS diffraction patterns obtained from Figure 1 (c and d) in the q_{xy} direction of screen-printed (a) control and (b) 4F-PEAFa PbI_2 thin films on SnO_2.

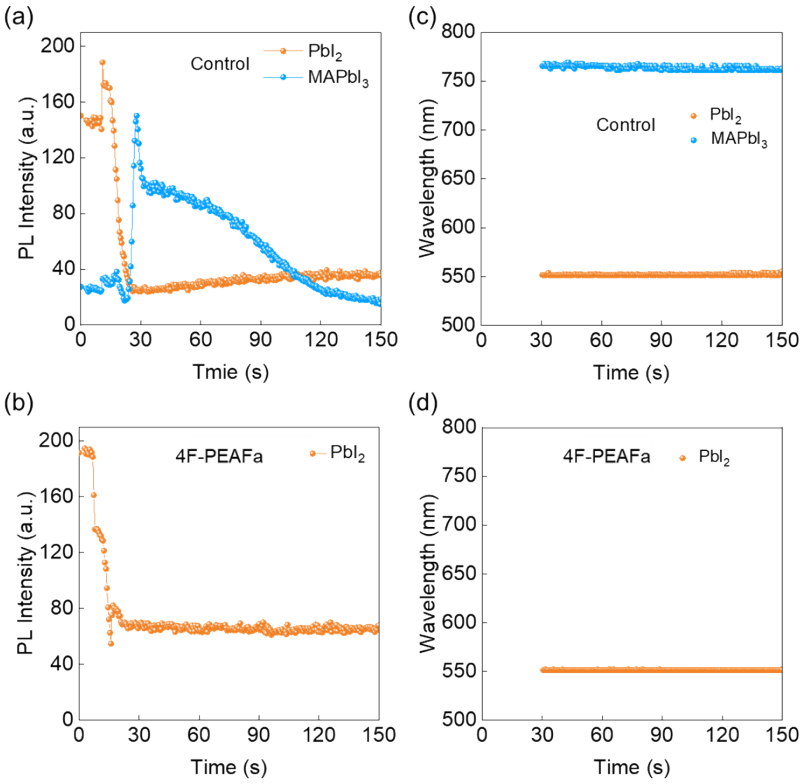

Fig. S3. Evolution of PL peak position for (a) control and (b) 4F-PEAFa PbI_2 thin films during the annealing process. PL intensity for (c) control and (d) 4F-PEAFa PbI_2 thin films during the annealing process.

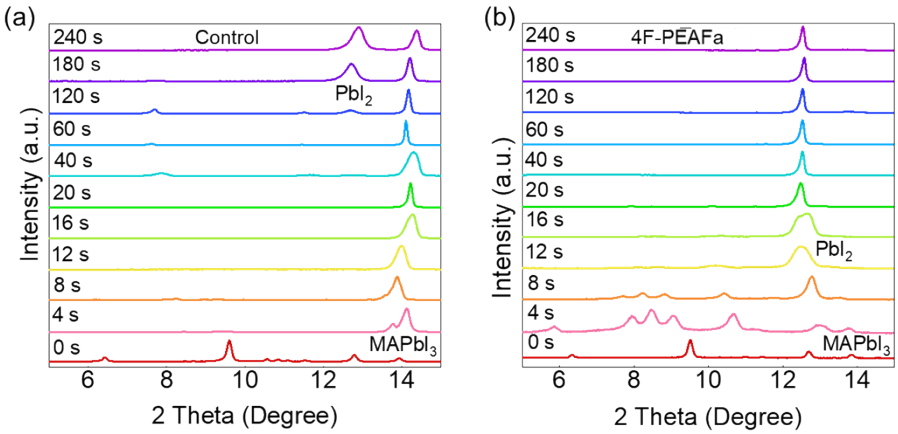

Fig. S4. In situ XRD patterns of (a) control and (b) 4F-PEAFa dried perovskite precursor inks on FTO/glass substrates.

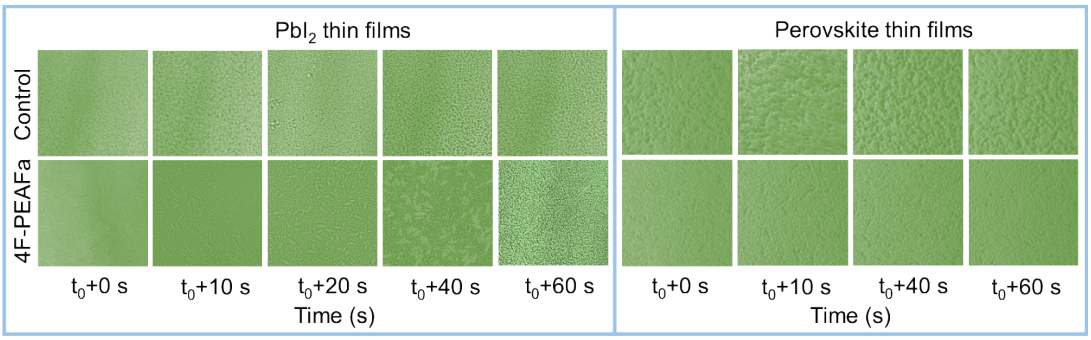

Fig. S5. The in situ optical microscopy of control and 4F-PEAFa PbI_2 and perovskite thin films.

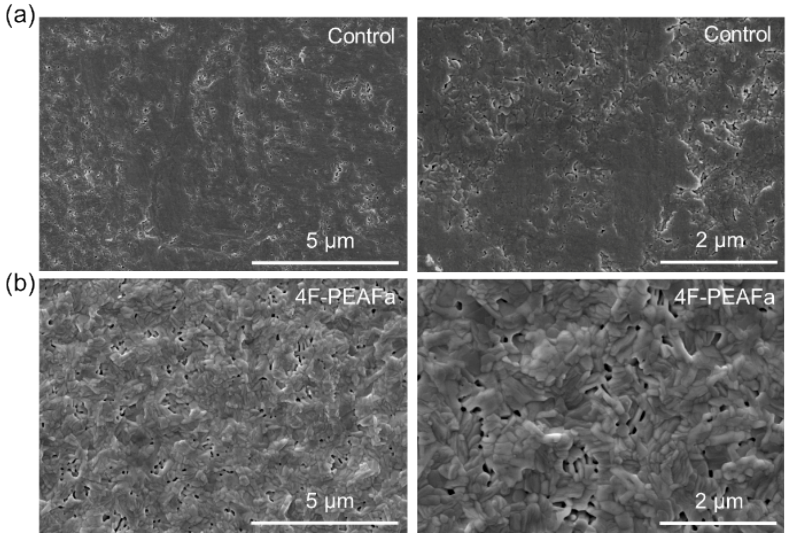

Fig. S6. The top-view SEM images of the (a) control and (b) 4F-PEAFa PbI_2 thin films.

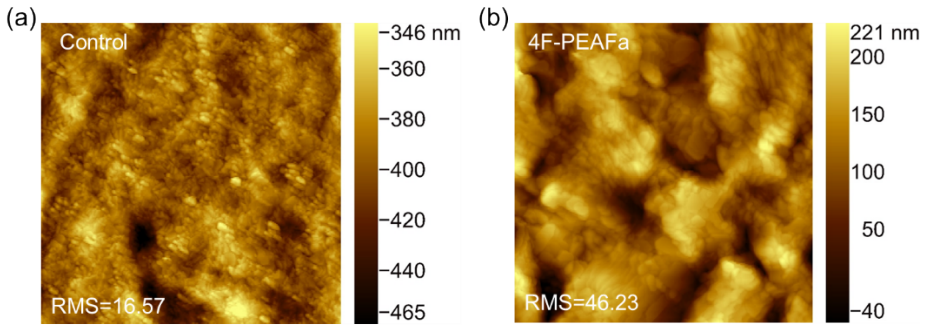

Fig. S7. AFM images of the (a) control and (b) 4F-PEAFa PbI_2 thin films.

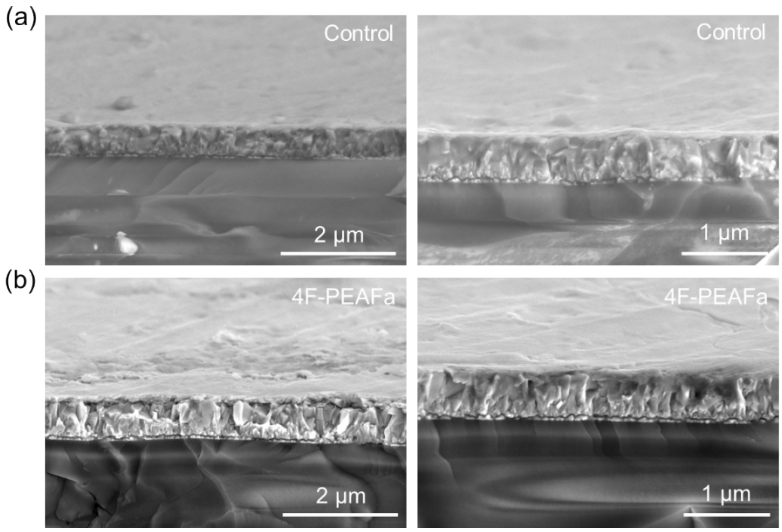

Fig. S8. The cross-sectional SEM images of the (a) control and (b) 4F-PEAFa PbI_2 thin films.

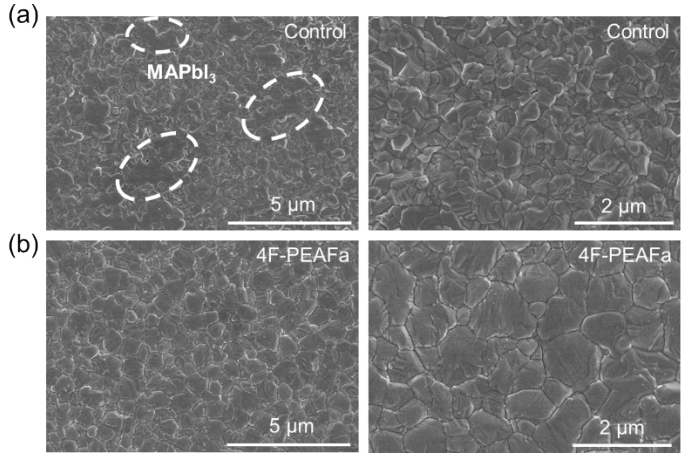

Fig. S9. The top view SEM images of the (a) control and (b) 4F-PEAFa perovskite thin films.

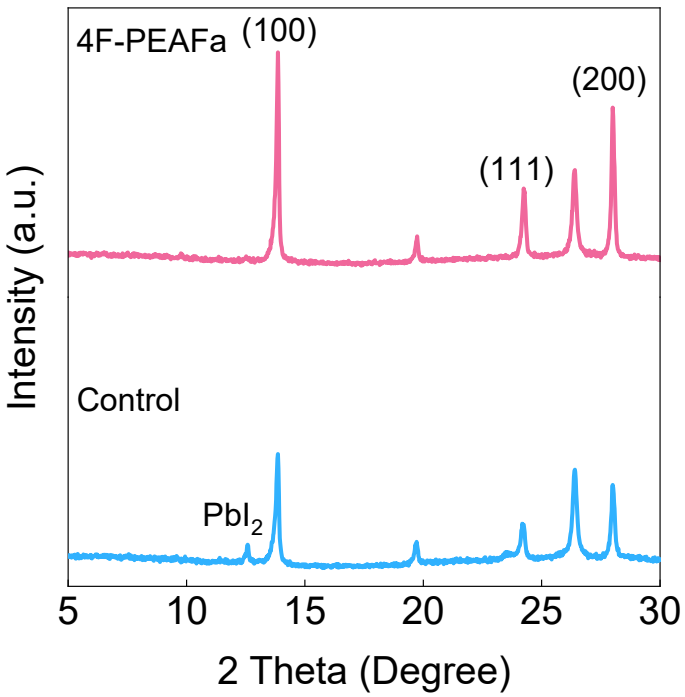

Fig. S10. XRD patterns of control and 4F-PEAFa perovskite thin films.

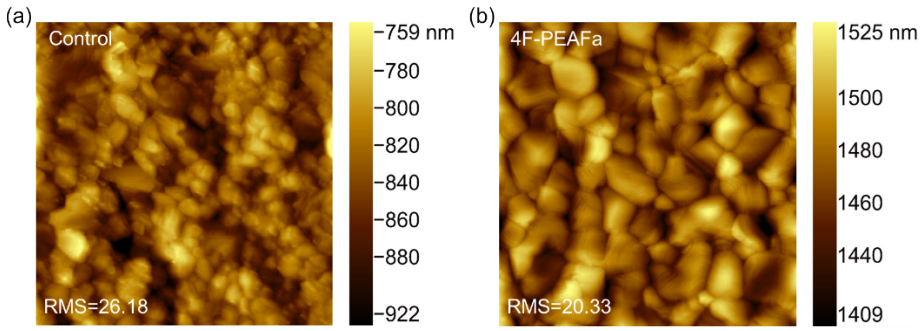

Fig. S11. AFM images of the (a) control and (b) 4F-PEAFa perovskite thin films.

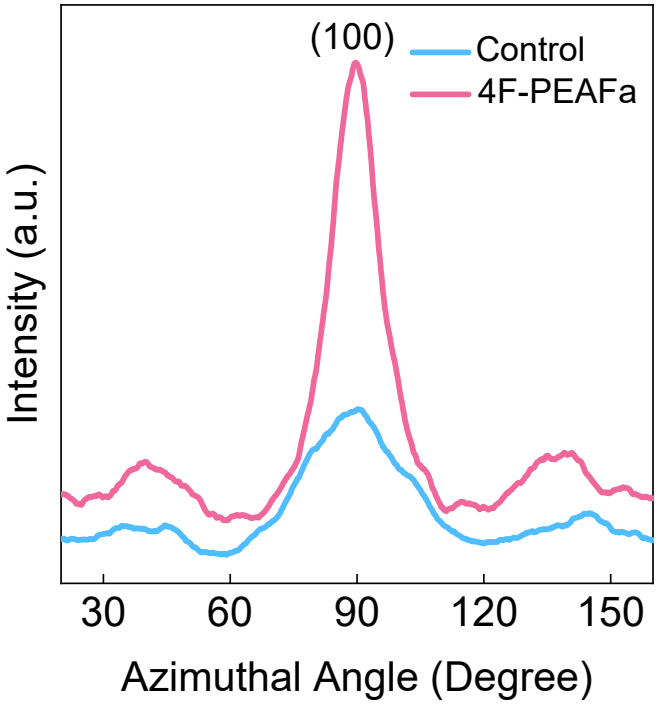

Fig. S12. Azimuth distribution map drawn by radial integral of the diffraction ring of the control and 4F-PEAFa perovskite thin films.

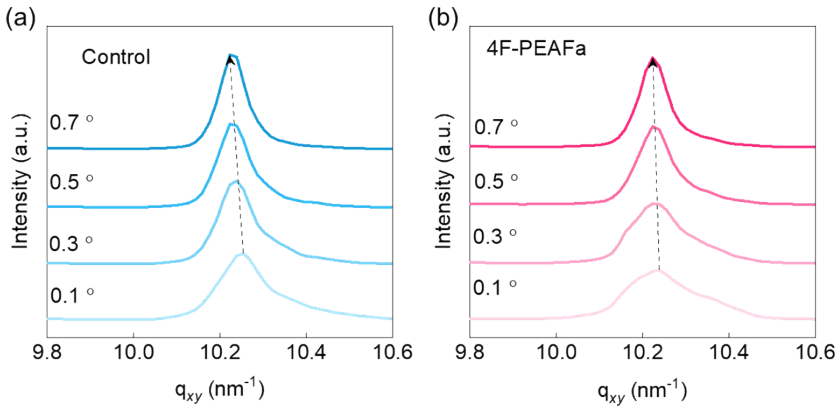

Fig. S13. The 2D GIWAXS curves of (a) control and (b) 4F-PEAFa perovskite thin films.

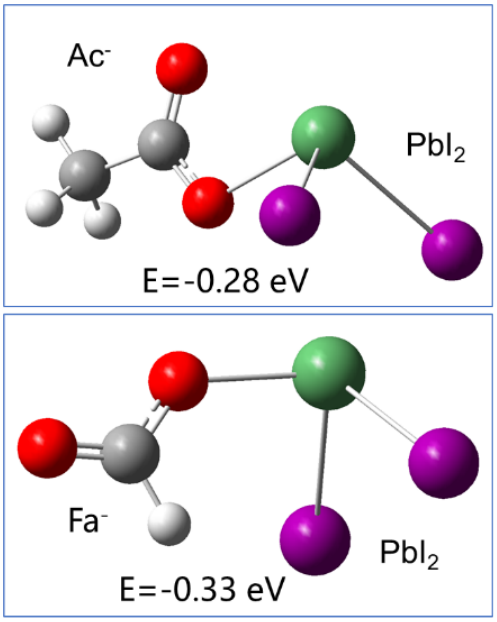

Fig. S14. The computational results of the binding energies between the PbI_2 molecule and Ac^- or Fa^-.

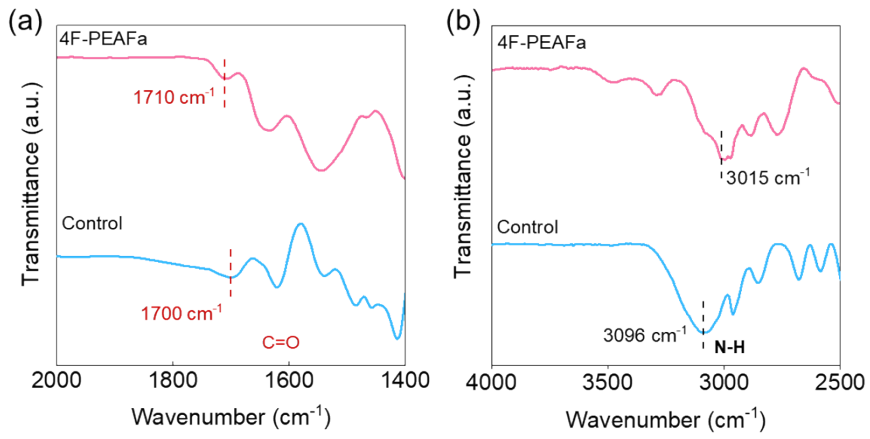

Fig. S15. FTIR spectra of the control and 4F-PEAFa PbI_2 inks.

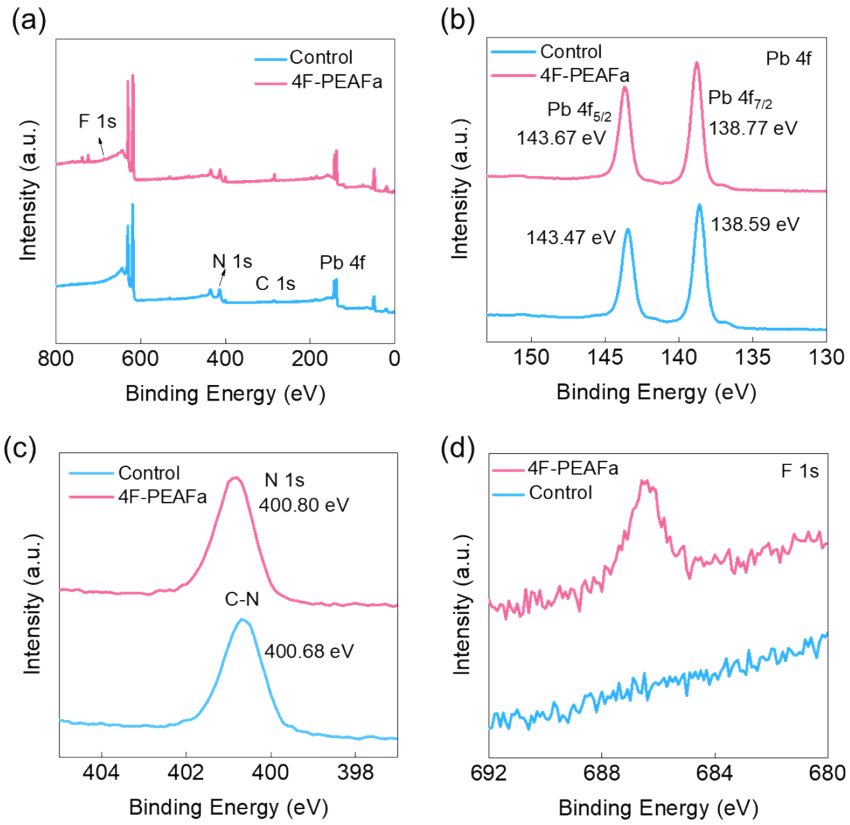

Fig. S16. (a) Full XPS spectra of the control and 4F-PEAFa perovskite thin films deposited in air. XPS spectra for (b) Pb 4f and (c) N 1s and (d) F 1s of the control and 4F-PEAFa perovskite thin films.

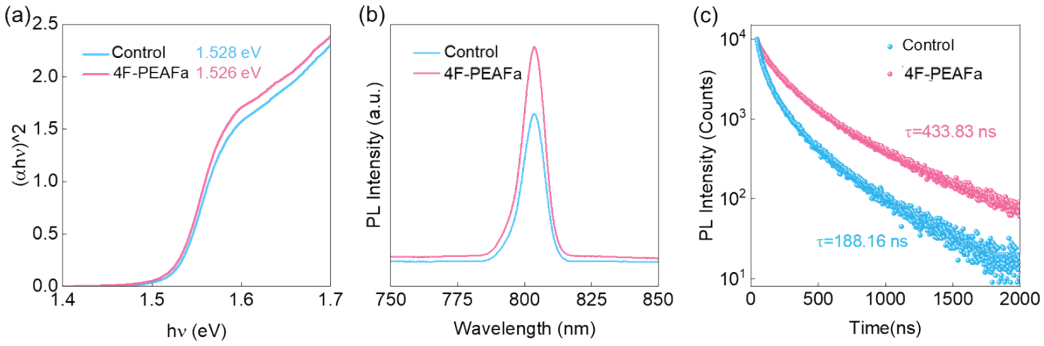

Fig. S17. (a) UV-vis absorption spectra of control and 4F-PEAFa perovskite thin films. (b) PL of control and 4F-PEAFa perovskite thin films. (c) TRPL spectra of control and 4F-PEAFa perovskite thin films.

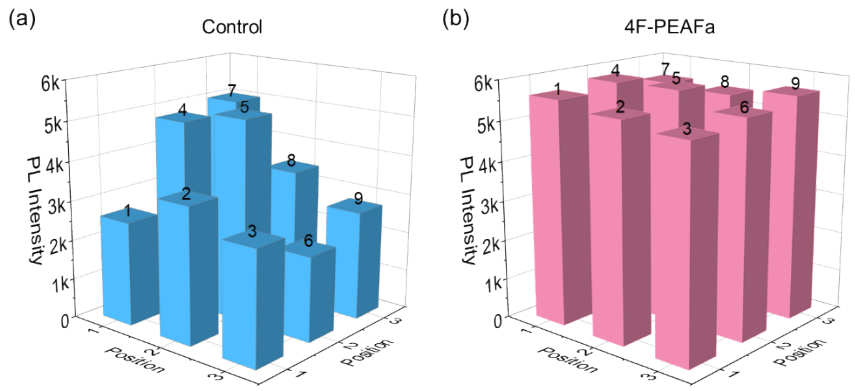

Fig. S18. PL intensity of 9 regions from (a) control and (b) 4F-PEAFa perovskite thin films (5 cm × 5 cm).

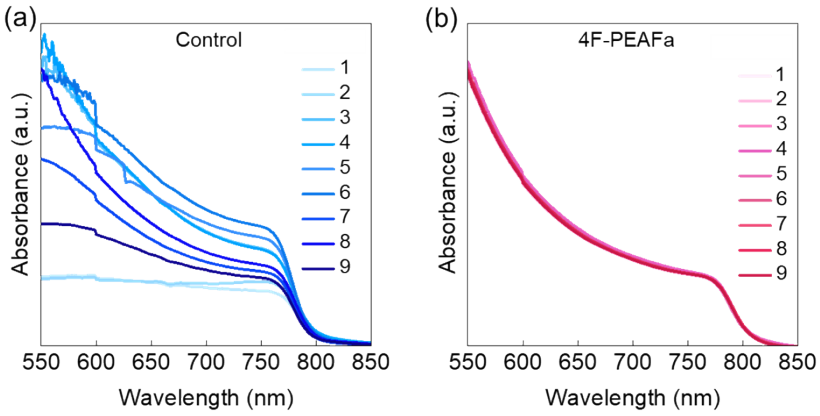

Fig. S19. UV-vis absorption spectra of 9 regions from (a) control and (b) 4F-PEAFa perovskite thin films (5 cm × 5 cm).

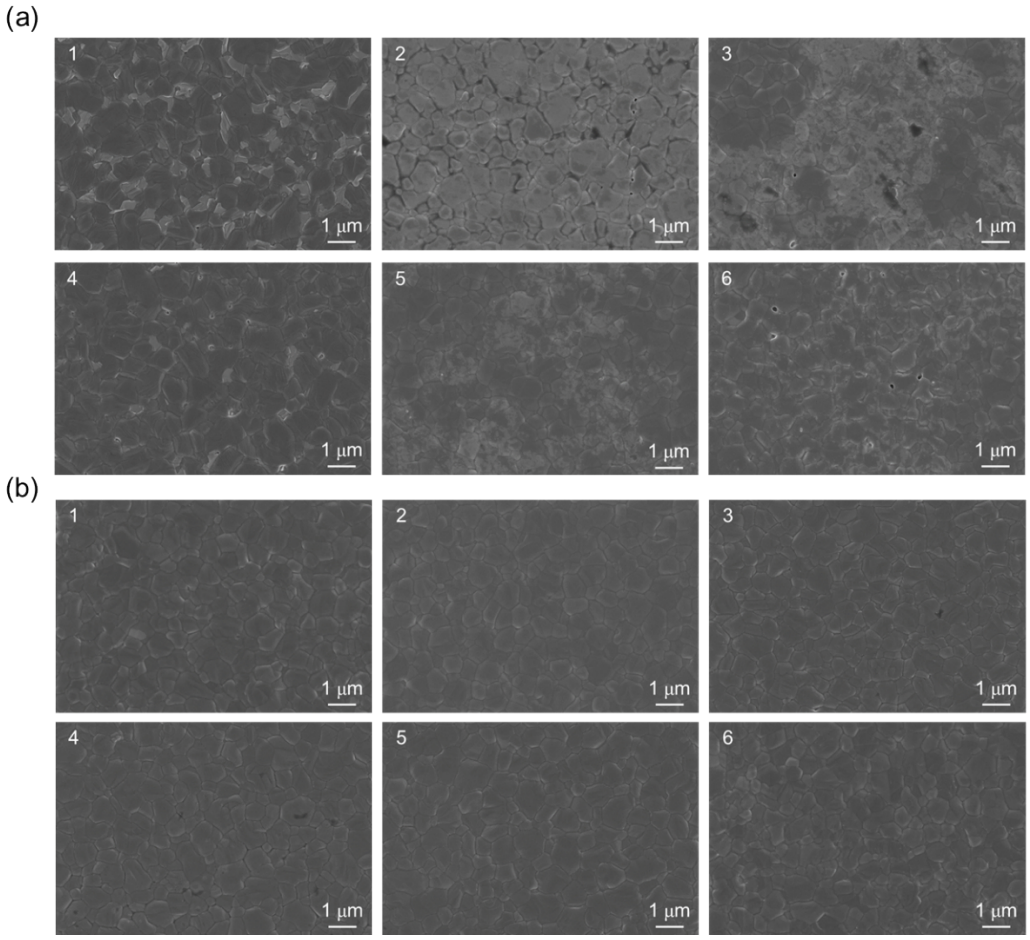

Fig. S20. Top-view SEM images of the six platforms in (a) control and (b) 4F-PEAFa perovskite thin films (5 cm × 5 cm).

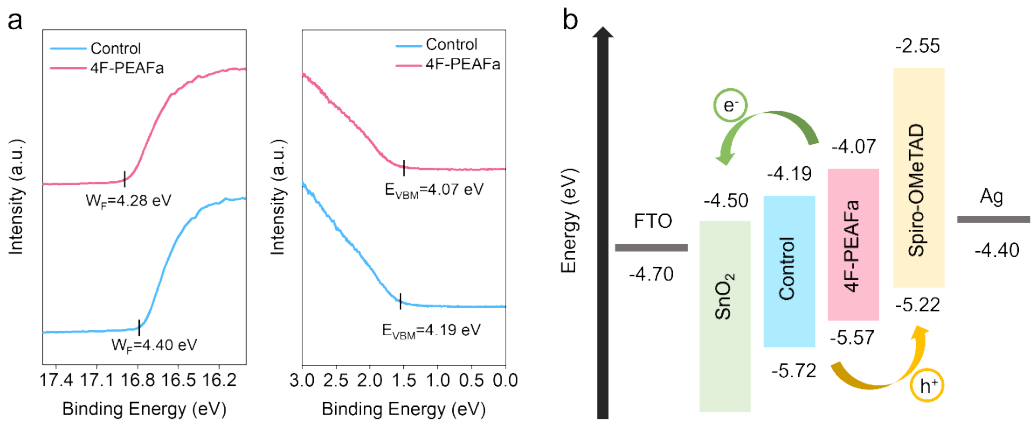

Fig. S21. (a) The ultraviolet photoelectron spectroscopy (UPS) spectra of control and 4F-PEAFa perovskite thin films. (b) The energy band structure of perovskite.

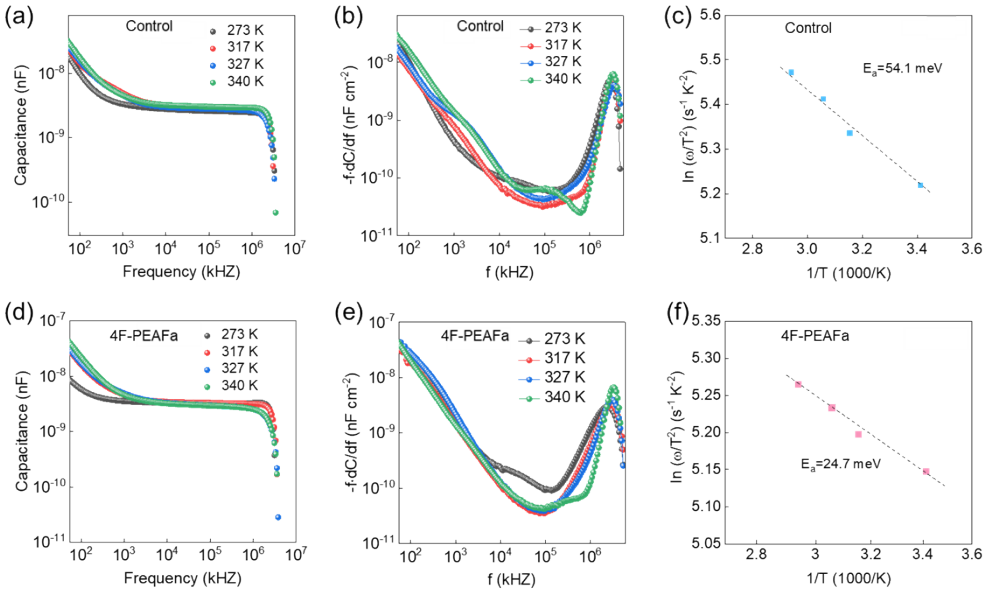

Fig. S22. The capacitance-frequency curves of (a) control and (d) 4F-PEAFa devices measured at different temperatures. The derivative specific capacitance (C) with respect to the frequency (*f*) of (b) control and (e) 4F-PEAFa devices at different temperatures. Arrhenius plot of (c) control and (f) 4F-PEAFa with the characteristic frequencies at different temperatures extracted from the derivative specific capacitance spectra.

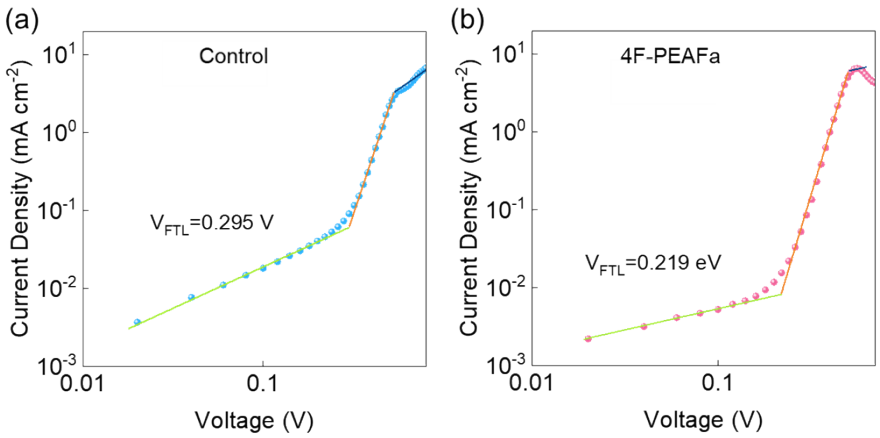

Fig. S23. V_{TFL} represents the trap-filled limit voltage. (a) Control device. (b) 4F-PEAFa device.

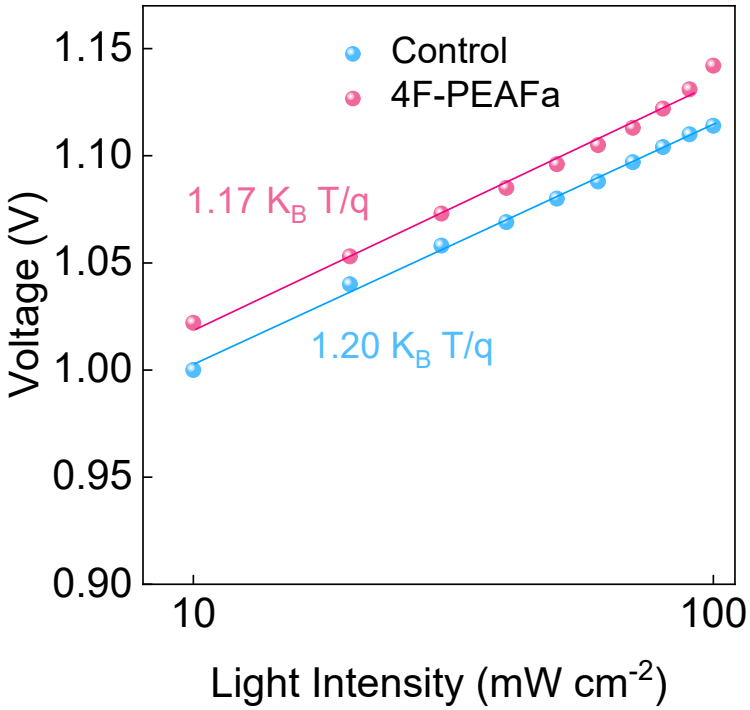

Fig. S24. Light intensity dependence of V_{OC} for the control and 4F-PEAFa devices. The ideality factor was calculated from the slope of the linear fit of the semilogarithmic plot.

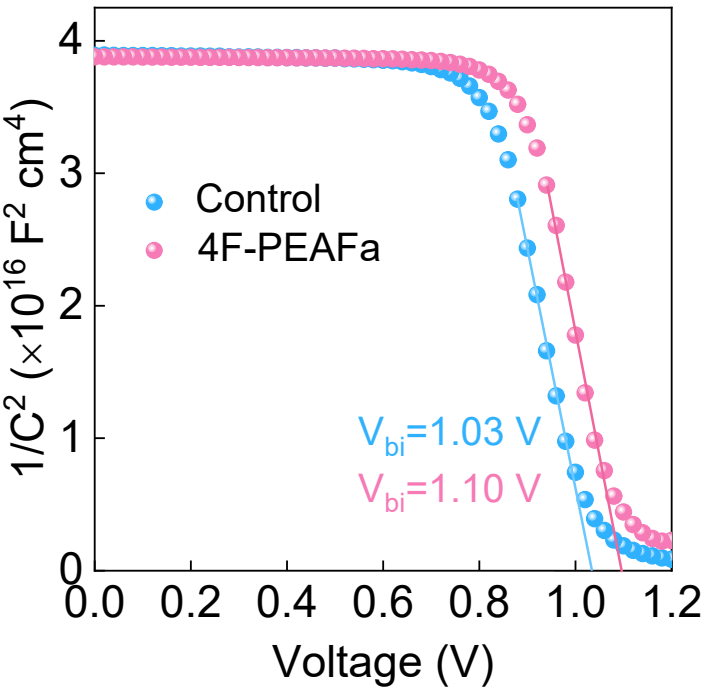

Fig. S25. Mott-Schottky plots of control and 4F-PEAFa devices, obtained under dark conditions.

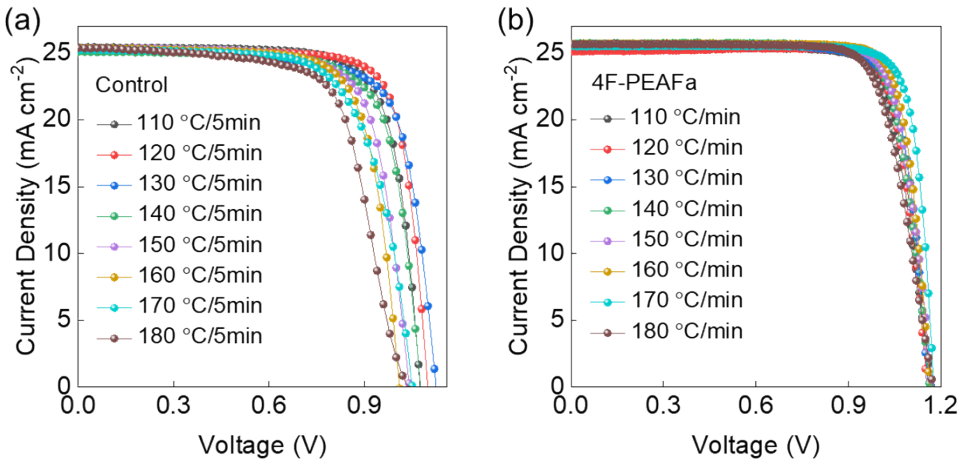

Fig. S26. *J-V* curves of control and 4F-PEAFa devices at different annealing temperatures. The photovoltaic parameters are summarized in Table S1 and S2.

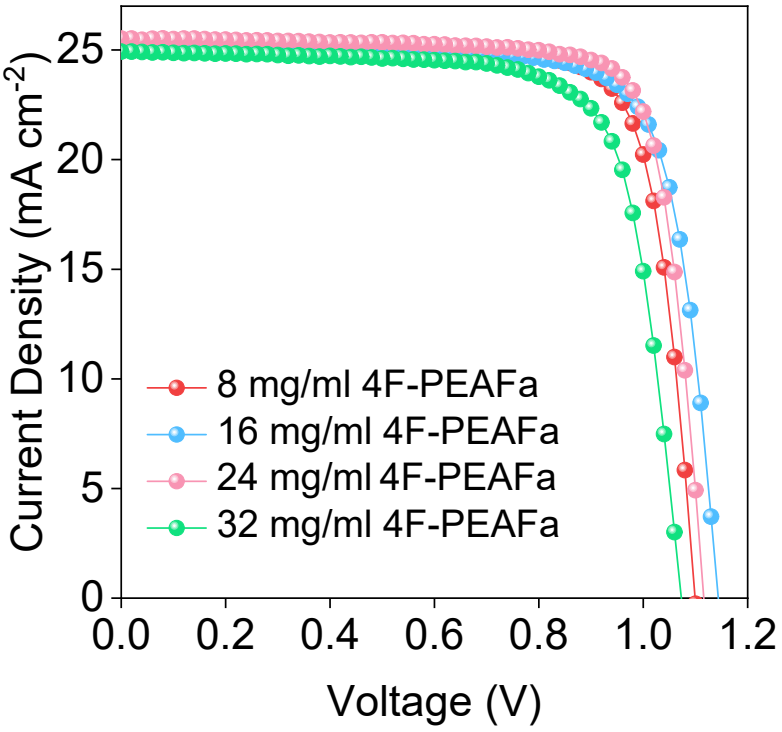

Fig. S27. *J-V* curves of 4F-PEAFa device with different concentrations. The photovoltaic parameters are summarized in Table S3.

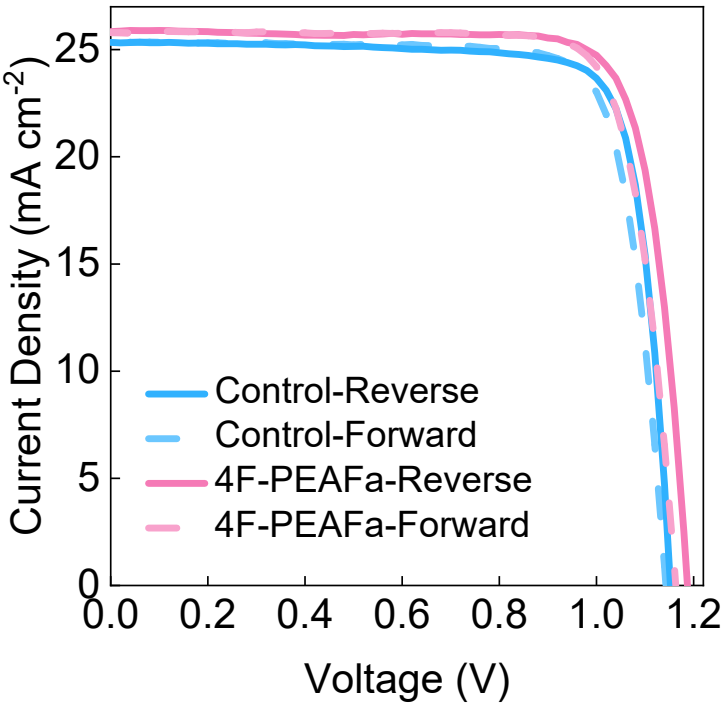

Fig. S28. *J-V* curves for reverse and forward scanning of control and 4F-PEAFa devices. The photovoltaic parameters are summarized in Table S5.

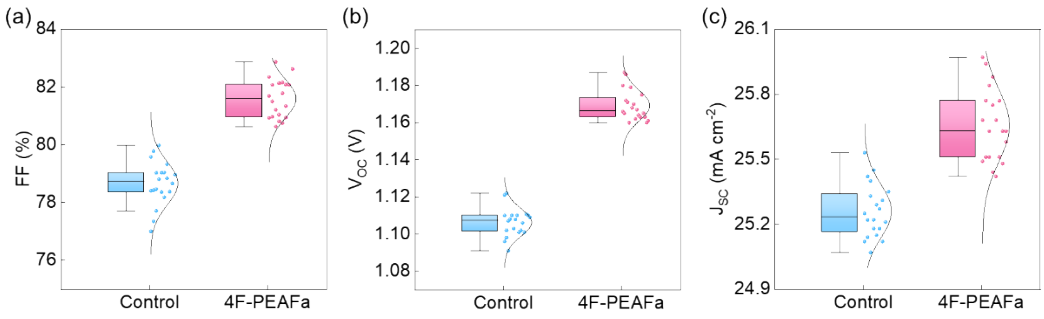

Fig. S29. Statistical (a) FF, (b) V_{OC} and (c) J_{SC} for control and 4F-PEAFa devices.

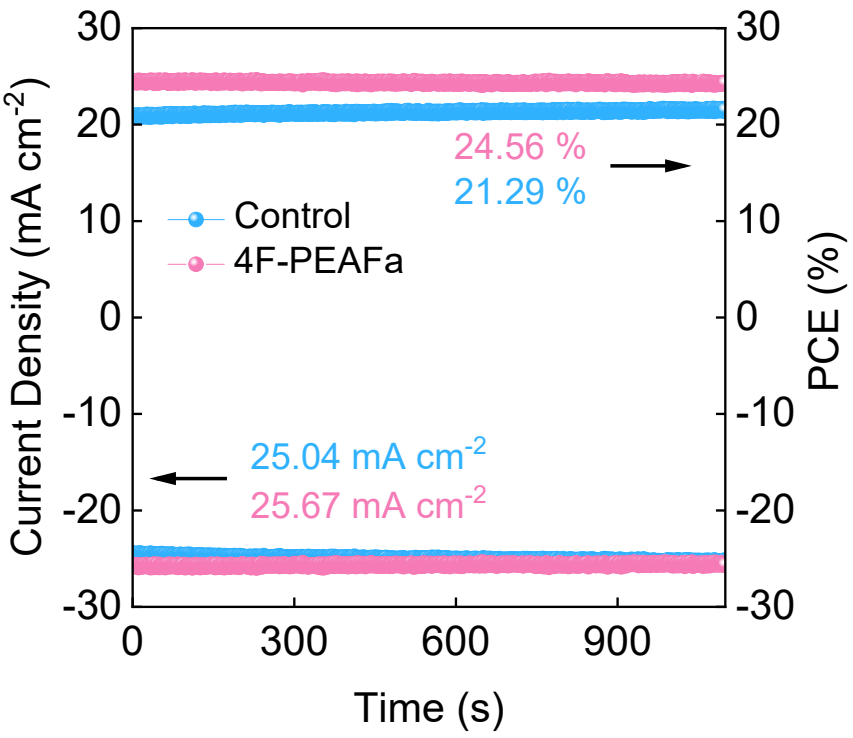

Fig. S30. Maximal steady-state photocurrent output of the control and 4F-PEAFa PSCs at MPP and the corresponding output powers.

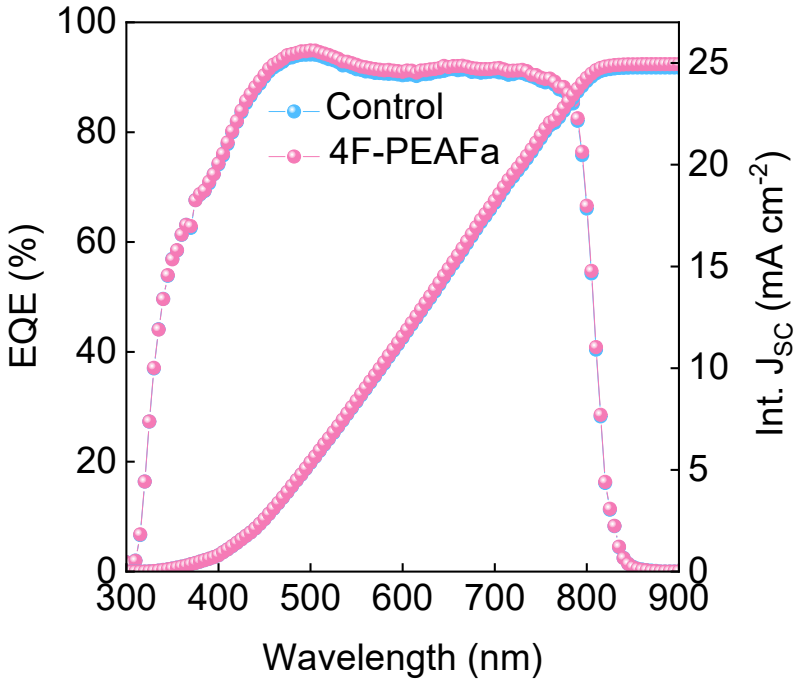

Fig. S31. The External Quantum Efficiency (EQE) Spectra and integrated J_{SC} of the control and 4F-PEAFa devices.

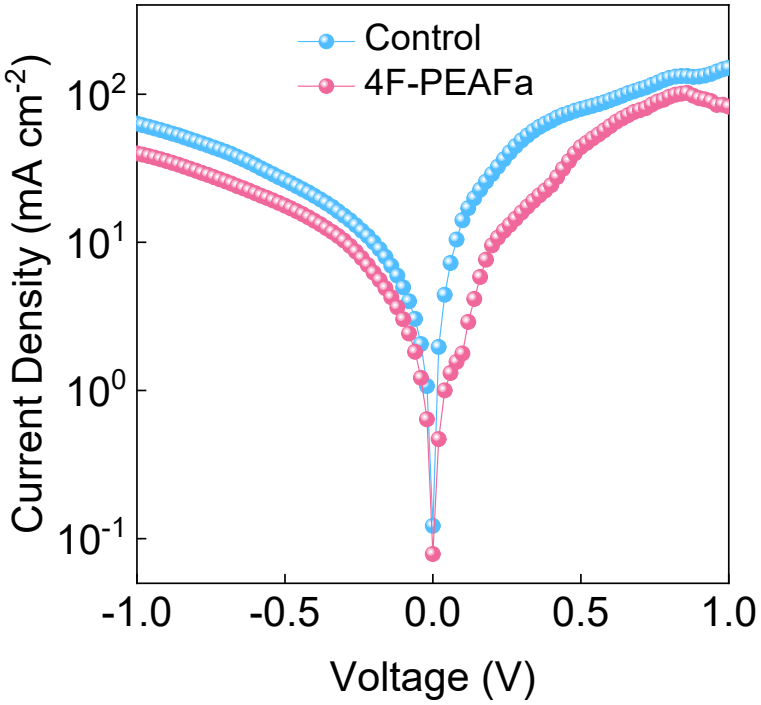

Fig. S32. Dark *J-V* curves of the control and 4F-PEAFa devices.

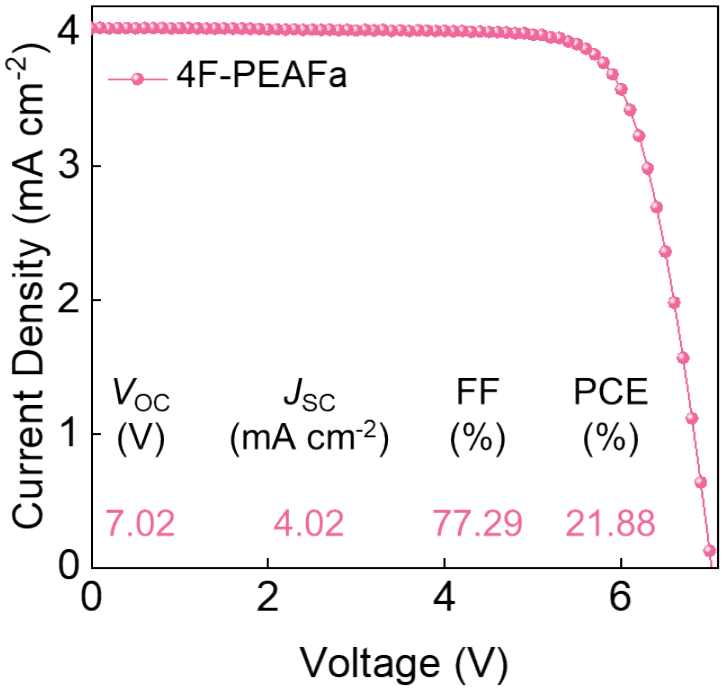

Fig. S33. *J-V* curves of the 4F-PEAFa PSM prepared by blade-coating.

Table S1. Photovoltaic parameters of control devices with different annealing temperatures/time.

Devices	V_{OC} (V)	J_{SC} (mA cm^{-2})	FF (%)	PCE (%)
110 ℃/5 min	1.07	25.43	76.31	20.96
120 ℃/5 min	1.10	25.27	78.62	21.84
130 ℃/5 min	1.12	25.17	74.68	21.15
140 ℃/5 min	1.08	25.05	74.72	20.16
150 ℃/5 min	1.04	25.36	73.85	19.50
160 ℃/5 min	1.01	25.33	74.47	19.13
170 ℃/5 min	1.05	25.23	69.22	18.43
180 ℃/5 min	1.03	25.35	67.13	17.64

Table S2. Photovoltaic parameters of control and 4F-PEAFa device with different annealing temperatures/time.

Devices	V_{OC} (V)	J_{SC} (mA cm^{-2})	FF (%)	PCE (%)
110 ℃/5 min	1.17	25.38	78.28	23.25
120 ℃/5 min	1.15	25.11	81.94	23.76
130 ℃/5 min	1.16	25.66	80.21	23.83
140 ℃/5 min	1.16	25.69	80.37	24.06
150 ℃/5 min	1.17	25.57	80.56	24.15
160 ℃/5 min	1.16	25.65	82.67	24.66
170 ℃/5 min	1.17	25.54	83.17	24.98
180 ℃/5 min	1.17	25.63	76.30	23.01

Table S3. Photovoltaic parameters of 4F-PEAFa devices with different concentrations.

Devices	V_{OC} (V)	J_{SC} (mA cm^{-2})	FF (%)	PCE (%)
8 mg/ml	1.10	25.30	84.51	23.52
16 mg/ml	1.15	25.27	85.44	24.83
24 mg/ml	1.12	25.32	83.71	23.74
32 mg/ml	1.09	25.00	83.04	22.63

Table S4. Photovoltaic parameters of the champion devices.

Devices	V_{OC} (V)	J_{SC} (mA cm^{-2})	FF (%)	PCE (%)
Control	1.11	25.36	78.05	22.01
4F-PEAFa	1.188	25.75	82.37	25.01

Table S5. Photoelectric parameters for reverse and forward scanning of control and 4F-PEAFa devices. The hysteresis index HI = $(PCE_{Reverse}-PCE_{Forward})/PCE_{Reverse}$ are also included.

Devices	V_{OC} (V)	J_{SC} (mA cm^{-2})	FF (%)	PCE (%)	Hysteresis Index (%)
Control-Reverse	1.12	25.11	77.38	21.82	5.7
Control-Forward	1.11	24.95	73.95	20.57	
4F-PEAFa-Reverse	1.18	25.84	80.62	24.74	2.1
4F-PEAFa-Forward	1.16	25.79	80.75	24.22	

Table S6. Photovoltaic parameters of the champion 4F-PEAFa modules (5 × 5 cm^2).

Devices	V_{OC} (V)	J_{SC} (mA cm^{-2})	FF (%)	PCE (%)
1	6.92	4	78.38	21.73
2	6.89	4.01	77.58	21.45
3	6.85	4.06	79.62	22.16
4	6.92	4.04	78.12	21.91
5	6.94	4.04	78.78	22.14
6	6.91	4.04	78.16	21.89
7	6.82	4.05	79.73	22.05
8	6.95	4.07	78.21	22.14
9	6.85	4.04	77.97	21.63
10	6.87	4.04	78.31	21.8
11	6.94	4.02	77.34	21.60
12	6.83	4.04	79.81	22.08
13	6.93	4.04	78.12	21.91
14	6.83	4.06	79.62	22.08
15	6.90	4.07	78.00	21.91
16	6.94	4.00	78.53	21.82
Average	6.88±0.06	4.035±0.35	78.57±1.24	21.8±0.35